General Disclaimer

One or more of the Following Statements may affect this Document

- This document has been reproduced from the best copy furnished by the organizational source. It is being released in the interest of making available as much information as possible.

- This document may contain data, which exceeds the sheet parameters. It was furnished in this condition by the organizational source and is the best copy available.

- This document may contain tone-on-tone or color graphs, charts and/or pictures, which have been reproduced in black and white.

- This document is paginated as submitted by the original source.

- Portions of this document are not fully legible due to the historical nature of some of the material. However, it is the best reproduction available from the original submission.

Produced by the NASA Center for Aerospace Information (CASI)

NASA TECHNICAL   NASA TM-78960
MEMORANDUM

NASA TM-78960

THE EFFECT OF FUEL-TO-AIR RATIO ON
BURNER-RIG HOT CORROSION

by Daniel L. Deadmore, Carl E. Lowell, and Fred J. Kohl
Lewis Research Center
Cleveland, Ohio
July 1978

INTRODUCTION

Hot corrosion is receiving increasing attention as an important failure mode of blades and vanes in gas turbines. Such failures are usually traced to airborne alkali chlorides from sea water combining with sulfur in the fuel during combustion to form sodium sulfate (Na_2SO_4). The sulfate condenses on the cooler parts of the turbine ($\sim900^\circ$ C) and causes a greatly accelerated attack. The accelerated attack is usually considered to be a combination of fluxing of the protective oxide with resultant accelerated oxidation and sulfidation with the attendant formation of liquid nickel sulfides (refs. 1 and 2).

Many types of tests have been developed for simulating this attack in the laboratory; one of the most common is the burner rig test. In this test, salt impurities are usually introduced as aqueous solutions of synthetic sea salt (largely NaCl) (ref. 3) into a combusion chamber where a sulfur-bearing fuel is burned with excess air. The resultant combustion gases are then directed through a nozzle at high velocity onto the test samples. Because of the assumption that liquid Na_2SO_4 is required for corrosion to occur, the test temperature is generally higher than the melting point of Na_2SO_4 (884° C) and lower than its dew point. The most commonly used test temperature is about 900° C which is near the temperature where the maximum rate of attack is observed. (refs. 1, 2, and 4).

Two major problems are associated with the interpretation of rig testing results: (1) the relationship between rig and engine results is not well established (ref. 5); and (2) enormous differences in results are obtained by rigs in different laboratories (ref. 6). The latter problem is especially important when comparing high gas velocity rig results which cover 200 to 800 meters per second (Mach 0.3 to Mach 1.0) with low velocity rig results at 6-30 meters per second. Another problem which is not often emphasized is the effect of pressure on hot corrosion; gas turbines commonly operate above ten atmospheres while the vast majority of burner rig tests are run at near ambient pressure. Thus, there is a need to determine the relationships between rig and turbine data and to understand the factors responsible for the differences among rigs.

An important step in the process of relating burner rig data to hot corrosion observed in gas turbine operation is to understand the effect of the test variables on hot corrosion in the burner rig. Previous work by two of the authors covered such variables as sample temperature, salt concentration, and salt composition (ref. 4). One of the tentative conclusions from this work was that the composition of the gases above condensed sulfate had a great effect on corrosion. Also, in a study of cooling hole plugging, the flame temperature (which is a function of fuel-to-air ratio) was found to be a key variable (ref. 7). As a result, the work reported herein was initiated to determine the effects of fuel-to-air ratio on hot corrosion as it directly effects both the flame temperature and the gas composition.

The approach used was to fix the sample temperature independently of the flame temperature by using an air-cooled hollow sample which was a cast vane alloy, Mar M-509. The fuel-to-air ratio was the variable as the sample temperature was fixed at 900° C. To further reduce complications, the corrodent was introduced as a single salt, sodium chloride (NaCl). Its rate of addition as an aqueous solution into the combustion chamber of a Mach 0.3 burner rig was fixed. Primary evaluation of the extent of attack was by measurement of metal loss as determined metallographically. In addition, scanning electron microscopy (SEM) and X-ray energy dispersive spectrometry (EDS) were used to evaluate the nature of the corrosive attack. Finally, thermodynamic calculations were made to estimate the combustion gas composition for the various fuel-to-air ratios.

THE ALLOY

The composition of Mar M-509 is given in table I, as taken from the vendor's certified analysis. The alloy is primarily a cobalt-chromium alloy with nearly ten weight percent nickel and over ten weight percent combined tungsten and tantalum. No other elements are present at a level greater than one weight percent although sufficient carbon (0.59 w/o) is available to allow the carbide strengtheners

to form. The as-received material as shown by its microstructure was a cobalt solid solution matrix with MC carbides at the grain boundaries as would be expected with this alloy (ref. 8). The alloy specimens were cast to the shape and size shown in figure 1 and all outer surfaces were glass bead blasted. The wall thicknesses varied from one part of the sample to the next but this variance caused no apparent problems.

PROCEDURES

The samples were cleaned, weighed and measured along the 1.6 mm dimension with a bench micrometer to a precision of ±2 μm. Figure 2 shows the test arrangement schematically. Air, fuel, and an aqueous solution of NaCl were injected into the combustor, ignited, and expanded through a covergent, divergent nozzle, exiting at about Mach 0.3. The NaCl concentration was fixed for all of the tests to give approximately 3 ppm Na in the flame. The fuel used was Jet-A $(CH_{1.9185})$ containing about 0.08 percent sulfur by weight. Fixed fuel-to-air mass ratios of between 0.033 and 0.050 were used. The actual flame temperatures were measured at the position of the sample using a sonic probe. For comparison, one run at the 0.033 and one at 0.050 fuel-to-air ratio were made without NaCl. The hollow sample was fixed in front of the exhaust gases with the long axis of the sample perpendicular to the nozzle axis and the blunt surface facing the flame. Cooling air flow through the sample was set to hold the hot zone at 900° C. After one hour the burner pivoted away and the sample was given a high velocity cold air blast for several minutes. Then the burner pivoted back and the cycle was repeated.

After one hundred cycles, the sample was removed, photographed, washed in distilled water, photographed, and weighed. The sample was then sectioned parallel to the ends in the center of the hot zone, mounted in epoxy, polished, and examined with the light microscope and SEM. Finally, metal recession measurements were made using the traveling microscope. Maximum attack values were used as in previous investigations (refs. 4 and 9). The metal recession values were estimated to be accurate to ±50 μm.

RESULTS AND DISCUSSION

External Appearance

The magnitude of the effect of fuel-to-air ratio on hot corrosion can be seen in figure 3. The exposed samples for the extreme values of fuel-to-air ratio in both oxidation and hot corrosion are shown slightly larger than life size. Slight evidence of attack can be seen on the higher fuel-to-air oxidation sample, but no attack can be observed on the other oxidation sample. However, the hot corrosion samples both show the effects of the salt attack to the unaided eye. Also quite apparent is the markedly greater attack in the sample run with a fuel-to-air ratio of 0.050 than that run at 0.033. The hot zone which encompasses the corrosion area is clearly discernible in each sample. No evidence of attack in cooler areas was seen on any of the samples.

Metallographic Analysis

As was expected from the outward appearance of the samples, very modest magnification is needed (see fig. 4) to judge the relative extent of attack. At this magnification (<8X) no attack of the oxidation samples can be discerned. The attack of the hot corrosion samples is quite obvious as is the relative attack under the different fuel-to-air ratios. At 0.033, the attack is definite but limited. In contrast the attack at 0.050 is so great that the 0.15 cm wall has almost been broached. Thus, fuel-to-air ratio has a major effect on hot corrosion. SEM and EDS, that permitted the use of higher magnification, were used in an attempt to elucidate any differences in the attack between the 0.033 samples and those run at 0.050 (see fig. 5). The micro-structures of the oxidation samples seem to confirm the impression gained from figure 3 that there was more attack on the sample run at 0.050 than that of 0.033 because the former has a thicker surface layer of oxide which contains some entrapped metal. This is, of course, not proof of greater attack as more of the layer from the 0.033 sample could have spalled upon cooling. To determine the extent of attack,

metal loss measurements must be made (see below). The outerlayer of both layers give the same EDS results: the major element was Ni with appreciable amounts of Cr, Co, and Ta.

The overall microstructure of the attack zones of the two hot corrosion samples shown in figure 5 definitely give a misleading impression. The 0.033 sample has a much greater depth of penetration than that of the 0.050 sample even though it is obvious from figure 4 and the thickness results below that the latter has lost much more metal. Both samples have three distinct zones labeled on figure 5 as I, II, and III. Zone III is the unaffected alloy and gives the same EDS information in both microstructures: Co, Cr, Ni, and Ta in order of creasing intensity.

The porous Zone II, which results from grain boundary attack of the MC carbides, is different for the two samples. Zone II of the high fuel-to-air ratio sample contains high Ta and Ni with almost no Cr and greatly reduced Co. In contrast, Zone II in the low fuel-to-air sample has slightly reduced Cr and slightly increased Ta as compared with the unaffected metal.

In the outermost layer, Zone I, similar differences to those found in Zone II were observed. The 0.050 sample had slightly more Ni than Co, and almost no Cr or Ta in Zone I while that of the 0.033 sample consisted almost exclusively of Co and with almost equal amounts of Cr. Thus, the effect of increasing fuel-to-air ratio seems to be to selectively increase the removal of Co and Cr. While loss of the Cr is certainly expected as Cr_2O_3 is the normal oxide formed, the loss of Co is more difficult to understand. One would expect, rather, that Ni would be the more likely element to be lost as nickel sulfides with low melting points are often found as a result of hot corrosion attack.

Metal Recession Measurements

As expected, the metal recession measurements reflect the enormous dependence of hot corrosion on fuel-to-air ratio (fig. 6). The dependence of oxidation on fuel-to-air, if present, is less than the esti-

mated accuracy of the measurements themselves. In contrast, the metal recession of the hot corrosion samples increases about 3 times over the range of fuel-to-air values investigated (0.033 to 0.050). The data have been connected by a straight line; however, it appears as though there might be some leveling off as a ratio of 0.050 is approached.

The shaded area of figure 6 covers the fuel-to-air values found in aircraft turbine combustion. Because these values are less than 0.030, an extrapolation of the data would indicate that the burner rig would be a more aggressive environment than an actual turbine in service. However, there is nothing to prevent a reversal in the curve at very low values; this might account for the cool corrosion phenomenon of greatly accelerated attack found by some investigators (refs. 10 and 11). This would be even more likely if the effect of the fuel-to-air ratio primarily results from the increased flame temperature, because the cool corrosion phenomenon seems to be associated with the lower flame temperatures found in flame tunnel types of rigs.

Just as there is no guarantee that the fuel-to-air/hot corrosion curve does not go through a minimum, it is possible the slope will differ for other alloys or other salt additions. As was shown in reference 4, different classes of alloys tend to respond to different hot corrosion variables in different ways. In addition, our unpublished data on samples run with salts containing Na, K, Ca, and Mg seem to have a fuel-to-air versus metal recession curve with pronounced but negative slope.

Thermodynamic Calculation of Combustion

Product Composition

Analysis of the deposits formed at all fuel-to-air ratios showed only Na_2SO_4, form III. Measurements of deposition rates as a function of fuel-to-air ratios indicated that, over the range of ratios used here, the deposition rate was constant within experimental error. It seemed, therefore, reasonable to assume that the differences in attack rate were due to changes in the composition of the gases over the deposit. With the use of a NASA/LeRC-developed computer program (ref. 12), the

equilibrium compositions of the combustion gases were calculated at
the calculated adiabatic flame temperature and at 200° C below this
temperature. Combustion gas temperatures measured at the position
of the sample were approximately 200° C lower than the calculated
adiabatic flame temperatures. While there is always a question of
whether or not equilibrium is reached under the burner rig conditions,
two recent papers give considerable confidence in the calculations being
a reasonable approximation of the experimental gas compositions.
Reference 13 compares calculated gas compositions with mass spec-
trometically measured values in an experimental burner and found good
agreement in residence times less than those calculated for the burner
rig. Reference 14 compared calculated dew points for Na_2SO_4 with
measured values found in the burner rig and also found good agreement.

The compositions of the gas phase as a function of fuel-to-air mass
ratio are plotted in figure 7. All species which mole fractions are
greater than 10^{-10} and thought to bear on hot corrosion are plotted.
Concentration levels of N_2, H_2O, Ar, OH, O, HO_2, NO, NO_2, N_2O,
and H_2 were not plotted. Over the range of fuel-to-air values used in
these experiments, the following species increased significantly with
increasing fuel-to-air ratio: $CO(10^3 X)$, $SO_2(2X)$, $HCl(1.5X)$, NaOH(1.5),
Na(80X), Cl(10X), NaO(30X). In contrast, the following species de-
creased: NaCl(10%), $SO_3(8X)$, $Na_2SO_4(10^5 X)$. Thus, the species normal-
ly associated with hot corrosion (i.e., gaseous NaCl and Na_2SO_4) de-
creased as the attack increased. In contrast, the species that are pre-
sent at higher concentrations as the environment becomes more aggres-
sive are CO, Na, NaO, and Cl.

To explain this dichotomy, at least two possibilities are evident -
the enormous increase in CO could cause local reducing conditions at
the sample or could indicate a potential for more carbon particle forma-
tion in the combustor; in either event, accelerated attack could be ex-
pected (refs. 15 and 16). The second possiblity is that the increased
Cl could accelerate the attack through the formation of volatile species
such as $(NaCl)_x CrO_3$ (ref. 17). The only certainty is that this effect
needs investigation on other alloys and with other salt compositions
before definite conclusions on the mechanisms can be made.

CONCLUSIONS

From the results obtained by the exposure of Mar M-509 to hot corrosion from NaCl impurities in the burner rig at various fuel-to-air ratios, the following conclusions have been drawn:

1. Fuel-to-air ratio has a major effect on hot corrosion; metal recession is three times greater at a fuel-to-air ratio of 0.050 than at 0.033. The increased recession appears to be due to loss of Cr and Co.

2. The mechanism causing the increase in attack is not clear, but it is related to changes in the combustion gas composition and not the composition of the salt deposit, which is always Na_2SO_4, nor the rate of deposition.

3. The fuel-to-air ratio must be taken into account when estimating turbine airfoil performance or when comparing results of one burner rig with those of another laboratory.

REFERENCES

1. Stringer, J.: Hot Corrosion in Gas Turbines. MCIC-72-08 Metals and Ceramics Information Center, 1972.

2. Stringer, J.: High Temperature Corrosion of Aerospace Alloys. AGARD-AG-200, Advisory Group For Aerospace Research and Development, Paris, 1975.

3. Substitute Ocean Water. Am. Soc. Test. Mater. Stand. D1141-75, 1975.

4. Deadmore, D. L.; and Lowell, C. E.: Burner Rig Alkali Salt Corrosion of Several High Temperature Alloys. NASA TM X-73659, 1977.

5. Page, K.; and Taylor, R. J.: Turbine Corrosion-Rig Evaluation and Engine Experience. Deposition and Corrosion in Gas Turbines, A. B. Hart and A. J. B. Cutler, eds., Halsted Press, 1973, pg. 350-375.

6. Hot Corrosion in Gas Turbines-Mechanisms, Alloy and Coating Development, Environmental Effects, and Evaluation. NMAB-260, National Materials Advisory Board, 1970. (Available from NTIS as AD-870745.)

7. Deadmore, D. L.; and Lowell, C. E.: Plugging of Cooling Holes in Film-Cooled Turbine Vanes. NASA TM X-73661, 1977.

8. Biss, V.: Phase Analysis of Standard and Molybdenum-Modified Mar-M509 Superalloys. J. Testing and Eval., vol. 5, May 1977, pp. 217-223.

9. Lowell, C. E.; and Deadmore, D. L.: Effect of a Chromium-Containing Fuel Additive on Hot Corrosion. NASA TM X-73465, 1976.

10. Wortman, D. J.; Fryxell, R. E.; and Bessen, I. I.: A Theory For Accelerated Turbine Corrosion at Intermediate Temperatures. Presented at the 3rd Conference on Gas Turbine Materials in a Marine Environment. (Bath, England), Sep. 20-23, 1976, Session V, paper 11.

11. Aprigliano, L. F.: Burner-Rig Simulation of Low-Temperature Hot Corrosion. MAT-77-68, Naval Ship Rec. & Dev. Center, 1977.

12. Gordon, S.; and McBride, B. J.: Computer Program for Calculation of Complex Chemical Equilibrium Compositions Rocket Performance, Incident and Reflected Shocks, and Chapman-Jouget Detonations. NASA SP-273 (1971).

13. Fryburg, G. C.; et. al.: Formation of Na_2SO_4 and K_2SO_4 in Flames Doped with Sulfur and Alkali and Carbonates. NASA TM-73794, 1977.

14. Kohl, F. J.; et. al.: Theoretical and Experimental Studies of the Deposition of Na_2SO_4 from Seeded Combustion Gases. NASA TM X-73683, 1977.

15. McKee, D. W.; and Romeo, G.: The Effects of Carbon Deposition on Hot Corrosion. Corrosion Problems in Energy Conversion and Generation, by C. S. Tedmon, Jr., ed., The Electrochemical Society, 1974, pp. 118-137.

16. Restall, J. E.: The Effect of Salt and Carbon Particles on the Degradation of Gas Turbine Materials. Presented at the 3rd Conference on Gas Turbine Materials in a Marine Environment, (Bath, England), Sep. 20-23, 1976, Session V, paper 10.

17. Fryburg, George C.; et. al.: Volatile Products in the Corrosion of Cr, Mo, Ti and Four Superalloys Exposed to O_2 Containing H_2O and Gaseous NaCl. J. Electrochem. Soc., vol. 124, no. 11, 1977, pp. 1738-1743. (also NASA TM X-73599, 1977.)

TABLE I. - COMPOSITION

OF MAR M-509

[All values in w/o.]

Cobalt	Balance
Nickel	9.90
Chromium	23.40
Tungsten	6.95
Tantalum	3.70
Titanium	0.28
Zirconium	0.46
Iron	0.32
Carbon	0.59
Boron	0.006
Sulfur	0.007
Silicon	<0.10
Manganese	<0.10
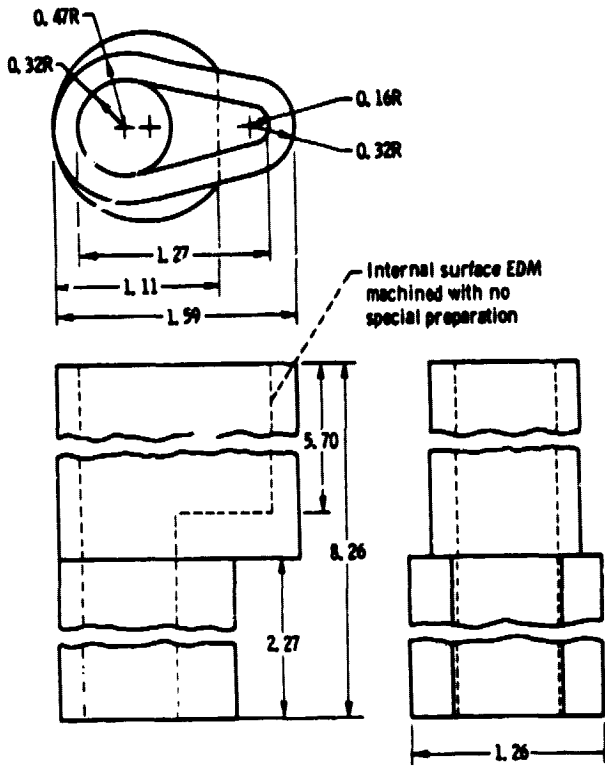
Figure 1. - Hollow erosion test bar (all dimensions in cm).
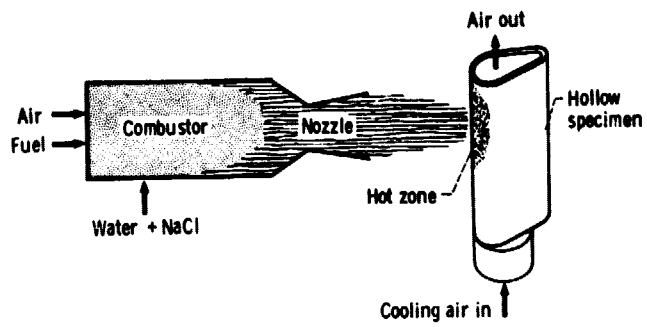
Figure 2. - Schematic diagram of burner rig.
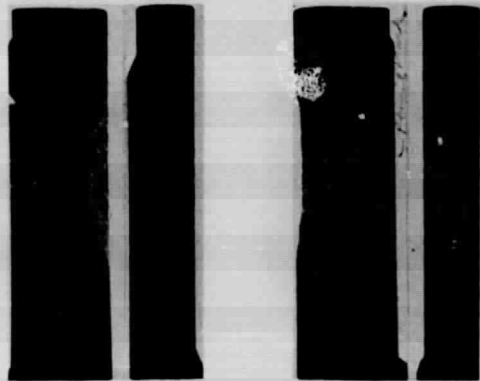
(a) 3 PPM Na AS NaCl, F/A = 0.033.

(b) 3 PPM Na AS NaCl, F/A = 0.050.
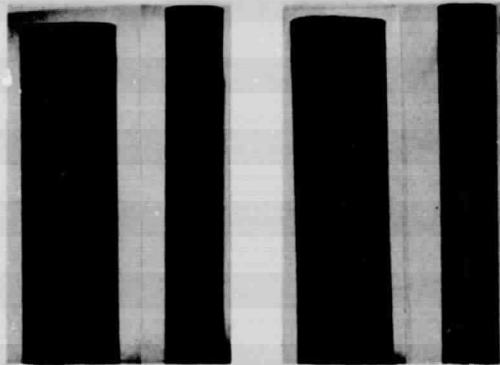
(c) OXIDATION ONLY, F/A = 0.033.

(d) OXIDATION ONLY, F/A = 0.050.

Figure 3. - Hot zone hot corrosion and oxidation of Mar M-509 as function of fuel-to-air ratio; 100 cycles of 1 hour at 900° C in Mach 0.3 burner rig; Jet-A fuel.

(a) 3 PPM Na AS NaCl, F/A = 0.033.

(b) 3 PPM Na AS NaCl, F/A = 0.050.

FLAME DIRECTION

3 µm
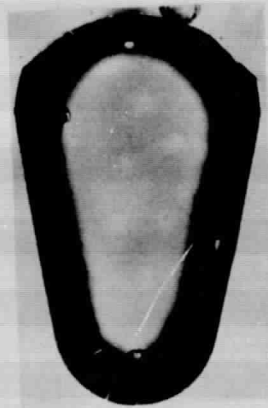
(c) OXIDATION ONLY, F/A = 0.033.

(d) OXIDATION ONLY, F/A = 0.050.

Figure 4. - Effect of fuel-to-air ratio on metal recession of Mar M-509; 100 cycles of 1 hour at 900° C in Mach 0.3 burner rig; Jet-A fuel.

(a) 3 PPM Na AS NaCl, F/A =
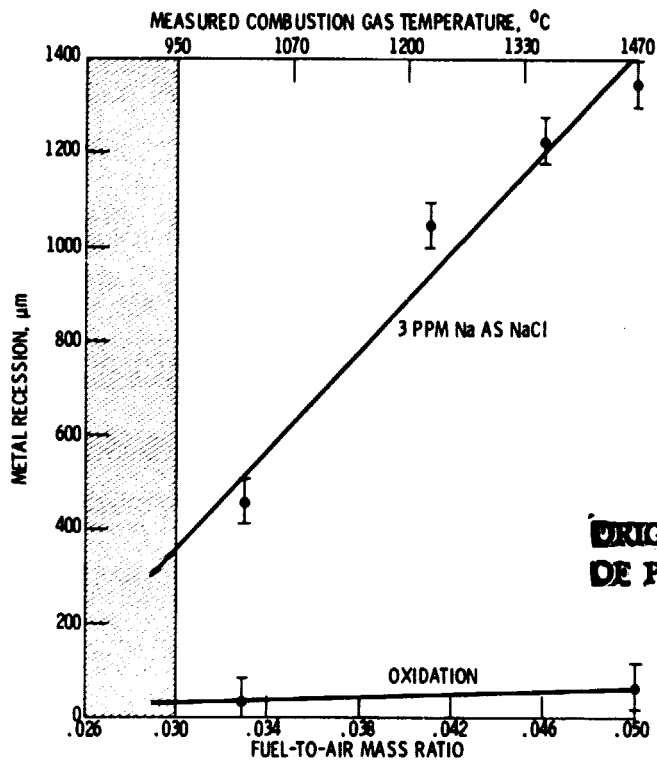0.033.
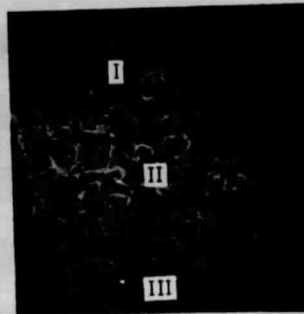
(b) 3 PPM Na AS NaCl, F/A =
0.050.

(c) OXIDATION ONLY, F/A =
0.033.

(d) OXIDATION ONLY, F/A =
0.050.

Figure 5. Effect of fuel-to-air ratio on microstructural degradation of
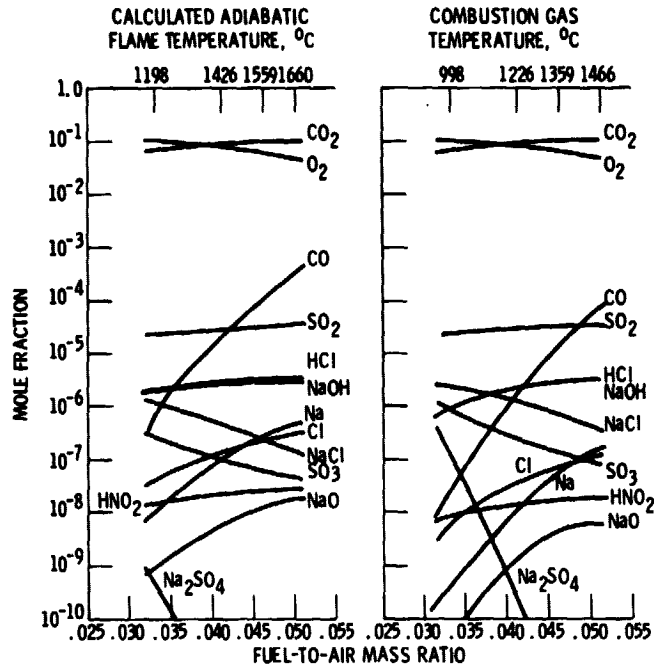Mar M-509; 100 cycles of 1 hour at 900^0 C in Mach 0.3 burner rig;
Jet-A fuel.

Figure 6. - Effect of fuel-to-air ratio on metal recession of Mar M-509; 100 cycles of 1 hour at 900° C in Mach 0.3 burner rig; Jet-A fuel. The shaded area covers fuel-to-air values found in aircraft turbine combustion.

CALCULATED ADIABATIC
FLAME TEMPERATURE, °C

COMBUSTION GAS
TEMPERATURE, °C

(a) CALCULATED COMBUSTION GAS COMPOSITION AS A FUNCTION OF FUEL-TO-AIR MASS RATIO AT THE CALCULATED ADIABATIC FLAME TEMPERATURE.

(b) CALCULATED COMBUSTION GAS COMPOSITION AS A FUNCTION OF FUEL-TO-AIR MASS RATIO AT TEMPERATURES 200° C BELOW THE ADIABATIC FLAME TEMPERATURE.

Figure 7.